scientific reports

Check for updates

OPEN

Numerical solution of an electrically conducting spinning flow of hybrid nanofluid comprised of silver and gold nanoparticles across two parallel surfaces

Aisha M. Alqahtani[1], Muhammad Bilal[2], Aatif Ali[3✉], Theyab R. Alsenani[4] & Sayed M. Eldin[5✉]

The analysis of the energy transport mechanism received much attention from scientists and researchers. Conventional fluids like vegetable oils, water, ethylene glycol, and transformer oil play a vital role in numerous industrial activities. In certain industrial operations, the low heat conductivity of base fluids causes significant difficulties. This inevitably led to the advancement of critical aspects of nanotechnology. The tremendous significance of nanoscience is in improving the thermal transfer process in different heating transmitting equipment. Therefore, the MHD spinning flow of hybrid nanofluid (HNF) across two permeable surfaces is reviewed. The HNF is made of silver (Ag) and gold (Au) nanoparticles (NPs) in the ethylene glycol (EG). The modeled equations are non-dimensionalized and degraded to a set of ODEs through similarity substitution. The numerical procedure parametric continuation method (PCM) is used to estimate the 1st order set of differential equations. The significances of velocity and energy curves are derived versus several physical parameters. The results are revealed through Tables and Figures. It has been determined that the radial velocity curve declines with the varying values of the stretching parameter, Reynold number, and rotation factor while improving with the influence of the suction factor. Furthermore, the energy profile enhances with the rising number of Au and Ag-NPs in the base fluid.

List of symbols

Au	Silver
B_0	Magnetic field
Ω	Angular velocity
NPs	Nanoparticles
T	Temperature
$(\rho c_p)_{hnf}$	Heat capacity
$(v_L > 0)$	Injection velocity
μ_{hnf}	Dynamic viscosity
λ	Stretching factor
q_r	Thermal radiative heat flux
β	Injection parameter

[1]Department of Mathematical Sciences, College of Science, Princess Nourah Bint Abdulrahman University, P. O. Box 84428, Riyadh 11671, Saudi Arabia. [2]Sheikh Taimur Academic Block-II, Department of Mathematics, University of Peshawar, Peshawar 25120, Khyber Pakhtunkhwa, Pakistan. [3]Department of Mathematics, Abdul Wali Khan University Mardan, Mardan 23200, Khyber Pakhtunkhwa, Pakistan. [4]Department of Electrical Engineering, College of Engineering in Al-Kharj, Prince Sattam Bin Abdulaziz University, Al-Kharj 11942, Saudi Arabia. [5]Faculty of Engineering, Center of Research, Future University in Egypt, New Cairo 11835, Egypt. ✉email: atifkh98@gmail.com; sayed.eldin22@fue.edu.eg

1

Re	Reynold number
R_0	Rotation constraint
$C_2H_6O_2$	Ethylene glycol formula
$f(\eta)$	Velocity profile
ϕ_{Ag}	Silver nanoparticles
Ag	Gold
L	Distance between surfaces
u, v, w	Components of velocity
k_{hnf}	Thermal conductivity
Q_0	Heat source
p	Pressure
ρ_{hnf}	Density
α	Suction parameter
σ_{hnf}	Electrical conductivity
$v_0 < 0$	Suction velocity
Rd	Radiation factor
Pr	Prandtl number
Mn	Magnetic term
EG	Ethylene glycol symbol
$\theta(\eta)$	Energy profile
ϕ_{Au}	Gold nanoparticles

Due to the theoretical and practical uses in medical, industrial, and engineering sectors, fluid flow between parallel surfaces has several applications, such as low-cost fabrication, food processing, centrifugal filtering processes, rotating apparatus, gas–solid fluidized beds, ease of multiplexing, and miniaturization. Researchers are still exploring new and exciting aspects of flow characteristics in a rotating frame between two parallel surfaces[1–3]. The magnetized hybrid nanofluid rotating flow between two surfaces featuring entropy formation was theoretically evaluated by Khan et al.[4]. Krishna et al.[5] described the time-varying sinusoidal pressure gradient and the slip effect on the magnetohydrodynamic (MHD) convective rotating flow. The findings show that the boundary layer thins out as the fluid motion is resisted by an elastic and magnetic field. A micropolar hybrid nanofluid's rotational flow and heat transference within the rotatable surface were addressed by Islam et al.[6]. The findings show that increasing magnetic parameter values raises the velocity curve. The 3D spinning flow of Jeffrey fluid was addressed by Fiza et al.[7] employing MHD and the Hall Current effect between two parallel surfaces. Heat transmission through magnetized rotational flow across an elastic sheet was addressed by Shahzad et al.[8]. Based on the findings, the rotational flow has a negative impact on heat transfer since it increases drag force. The MHD nanofluid flow was assessed by Bilal et al.[9]. A hybrid nanofluid's rotational squeezing flow between two parallel surfaces with entropy formation was analyzed by Ali et al.[10]. The features of the hydromagnetic radiative HNF rotating flow between the two shrinking discs were investigated by Yaseen et al.[11]. The upshot of MHD on the entropy optimization of nanofluid rotational flow over a spinning disc was observed by Alqarni et al.[12]. The MHD Casson nanoliquid flow was discussed by Alqahtani et al.[13] over an elongating surface. A permeable medium was employed by Ramzan et al.[14] to evaluate the hydrodynamic and thermal radiation features of the rotating flow of two distinct water-based hybrid nanofluids with the variation of particle sizes. Some related studies may be found in Ref.[15–18].

The formation of a hybrid nanofluid is accomplished by combining two distinct kinds of NPs with the base fluid. When nanoparticles are appropriately dispersed, hybrid nanofluids can provide substantial benefits in addition to their anomalously high thermal conductivity. Numerous engineering industrial sectors, including microelectronics, manufacturing, microfluidics, medicine, etc. can benefit from the application of hybrid nanofluids for heat transmission[19]. Gul et al.[20] reported a computational study to investigate the HNF flow over an enlarging surface. Due to its effective thermophysical behavior, nanoliquid performs more effectively than basic nanofluids. Tlili et al.[21] evaluated the magnetized HNF flow across an elongating surface with slip effects and non-uniform thickness. The results demonstrate that hybrid nanofluids are more resistant to the effects of the Lorentz force than nanofluids. Considering blood as a base fluid, Manzoor et al.[22] calculated the energy communication through HNF with magnetic dipole characteristics over a scattering sheet. Wahid et al.[23] analyzed the flow of a Marangoni HNF across an implanted infinitely permeable disc. Waqas et al.[24] scrutinized the consequence of thermal radiations on HNF flow as it passed through a revolving disc. Kumar et al.[25] described the heat transport through HNF flow along a stretchy cylinder. In a squeezed channel using engine oil as base fluid, Chu et al.[26] reported an unsteady viscous fluid flow of gold-silver hybrid nanofluid of irregular configurations. The findings show that hybrid nanoparticles perform better than nanofluids. Forced convection in a 3D heat sink was analyzed numerically by Wang et al.[27]. The upshot of heat generation and thermal conduction on the flow of ferromagnetic HNF through a permeable substrate with slip effects were studied by Eid and Nafe[28]. It is observed from the result that increased hybrid nanoparticle concentration improves heat transfer in a shrinkable container. Alqahtani et al.[29] estimated the impact of the slip effect and varying thickness on 3D HNF stagnation point flow along a stretchy heated curved cylinder. Tayebi et al.[30] documented the thermal convection of an Al2O3/H2O nanoliquid contained between two rotating cylinders. Chamkha et al.[31] used the numerical approach to analyze the MHD HNF in a closed container under the impact of the shape of nanomaterials and thermal radiation. The results showed that the local Nusselt numbers are more significantly affected by laminar nanomaterials than by other nanomaterial shapes. Seyyedi et al.[32] used a numerical algorithm to resolve the entropy generation and heat transfer evaluations for a hexagonal cavity filled with Cu-H2O nanofluid and exposed to an aligned magnetic

field. The findings showed that, for greater values of magnetic factor, the Nusselt numbers increases. Some further related studies may be found in Ref.[33–40].

The influence of magnetism on magnetic materials, electric currents, and moving electric charges, is characterized by a vector field known as the magnetic field. Hannes Alfven first brought the concept of magnetohydrodynamics (MHD) to the world in 1970. Magnetically forced electrical conductivity in fluids is the focus of MHD. Electrolytes, plasmas, and liquid metals are all examples of materials with magnetic moments. Many different fields, including astronomy, geophysics, aviation, electromagnetic pumping, plasma jets, and MHD power generation, have found usage for MHD[41]. Alotaibi et al.[42] calculated the impact that thermal absorption and injection have on the magnetohydrodynamic behavior of a fluid flow of Casson nanofluid in a boundary layer across a non-linear stretched surface. The 3-dimensional incompressible MHD models with magnetic diffusion and partial dissipation were analyzed by Wu and Zhu[43]. Armaghani et al.[44] reviewed the impact of the location and size of the source and sink of heat on MHD mixed convection in the hybrid nanofluid within the L-shaped cavity. The results show that the most power applied to the sink yields the most efficient heat transmission. Patil et al.[45] and Elayarani et al.[46] reported the unsteady 2D nanoliquid flow containing gyrotactic micro-organisms. Vishalakshi et al.[47] and Khashi'ie et al.[48] evaluated the magnetized flow of HNF across a revolving plate with the Joule heating effect. According to the outcomes, an increase in the magnetic effect makes heat transmission more efficient. Abdelhameed[49] examined how the existence of MHD and the porosity of sodium-alginate fluid affected the formation of entropy. It is noted from the result that the Bejan number effect the velocity curve. Kodi and Mopuri[50] inspected the MHD HNF flow across a permeable substrate with a chemical reaction.

As we have discussed that the analysis of energy transport mechanism received much attention among scientists and researchers. But in certain industrial operations, the low heat conductivity of base fluids causes complications. The tremendous significance of nanoscience is in improving the thermal transfer process in different heating transmitting equipment. Therefore, the present work aims to assess the MHD spinning flow of an EG-based HNF across two permeable surfaces. The hybrid nanofluid is made of Ag-NPs, Au-NPs, and ethylene glycol. The flow mechanism is studied under the impact of a constant magnetic field. The numerical procedure PCM is used to estimate the 1st order set of ODEs. The significances of velocity and energy curves are derived versus several physical parameters.

Mathematical formulation

We have assumed steady and an incompressible HNF flow across two parallel surfaces, apart from each other at a distance of L. The conducting hybrid nanoliquid comprised of silver (Ag) and gold (Au) nanoparticles are perpendicularly exposed to the constant magnetic field (B_0) in the y-direction. The parallel surfaces are considered porous and allow injection & suction. Both surfaces (upper at $y = L$ and lower at $y = 0$) are stretching with the velocity bx & ax as exposed in Fig. 1. The system (surfaces and fluid) rotates with an angular velocity (Ω) in the y-axis. The flow is mathematically expressed as[51,52]:

$$\frac{\partial u}{\partial x} + \frac{\partial v}{\partial y} = 0,$$ (1)

$$u\frac{\partial u}{\partial x} + v\frac{\partial u}{\partial y} + 2\Omega w = -\frac{1}{\rho_{hnf}}\frac{\partial p}{\partial x} + \left(\frac{\mu_{hnf}}{\rho_{hnf}}\right)\left(\frac{\partial^2 u}{\partial x^2} + \frac{\partial^2 u}{\partial y^2}\right) - \frac{\sigma_{hnf}B_0^2}{\rho_{hnf}}u,$$ (2)

$$u\frac{\partial v}{\partial x} + v\frac{\partial v}{\partial y} = -\frac{1}{\rho_{hnf}}\frac{\partial p}{\partial y} + \left(\frac{\mu_{hnf}}{\rho_{hnf}}\right)\left(\frac{\partial^2 u}{\partial x^2} + \frac{\partial^2 u}{\partial y^2}\right),$$ (3)

$$u\frac{\partial w}{\partial x} + v\frac{\partial w}{\partial y} - 2\Omega u = \left(\frac{\mu_{hnf}}{\rho_{hnf}}\right)\left(\frac{\partial^2 w}{\partial x^2} + \frac{\partial^2 w}{\partial y^2}\right) - \frac{\sigma_{hnf}B_0^2}{\rho_{hnf}}w,$$ (4)

$$u\frac{\partial T}{\partial x} + v\frac{\partial T}{\partial y} = \frac{k_{hnf}}{(\rho C_p)_{hnf}}\left(\frac{\partial^2 u}{\partial x^2} + \frac{\partial^2 u}{\partial y^2}\right) - \frac{1}{(\rho C_p)_{hnf}}\frac{\partial q_r}{\partial y} + Q_0(T - T_\infty).$$ (5)

The boundary conditions are:

$$\begin{aligned} u = ax, \ v = v_0, \ w = 0, \ T = T_0 \quad \text{at } y = 0, \\ u = bx, \ v = v_L, \ w = 0, \ T = T_L \quad \text{at } y = L, \end{aligned}$$ (6)

here x & y represent the rectangular coordinate, u, v, w are the components of velocity, k_{hnf} is the thermal conductivity, $(\rho c_p)_{hnf}$ is the heat capacity. ρ_{hnf} is the density and σ_{hnf} is the electrical conductivity, q_r is the thermal radiative heat flux, Q_0 is the heat source, p is the pressure, ($v_L > 0$) is the injection velocity at the upper surface and $v_0 < 0$ is the suction velocity at the lower surface.

The following transformations are used:

$$u = axf'(\eta), \ v = -aLf(\eta), \ w = axf(\eta), \ \theta = \frac{T - T_L}{T_0 - T_L}, \ \eta = \frac{y}{L}.$$ (7)
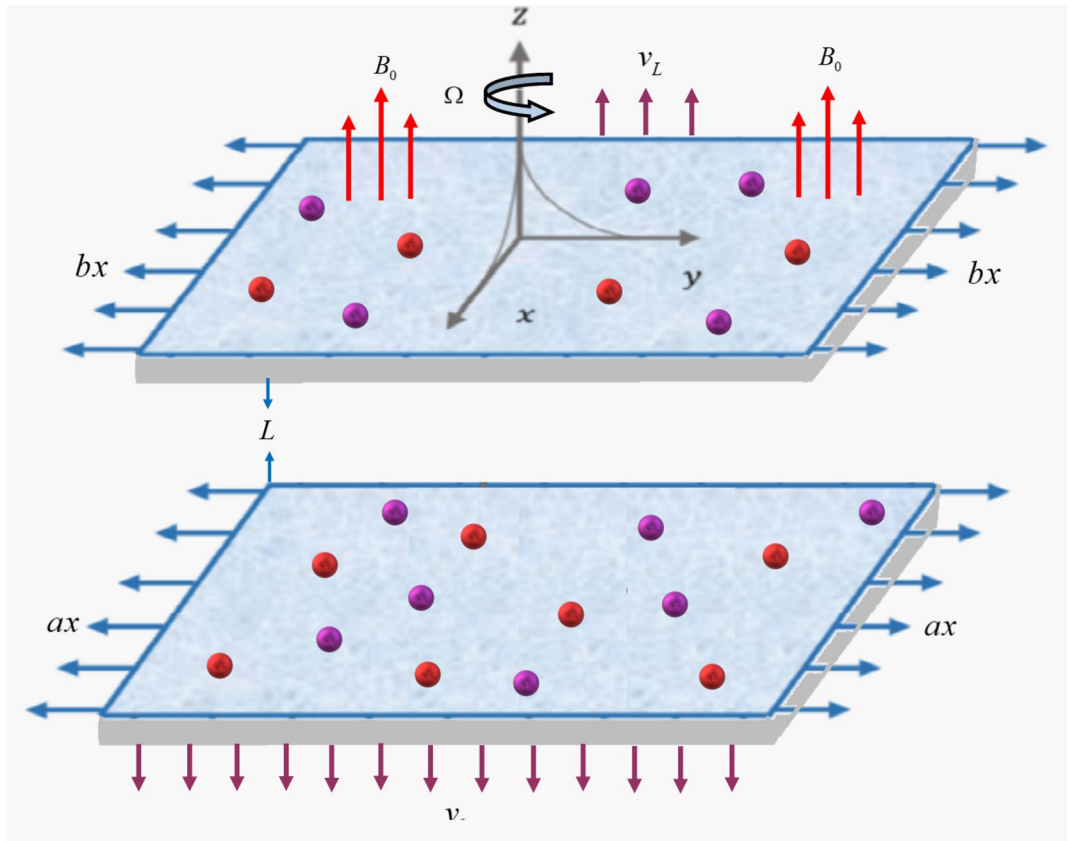
Figure 1. Hybrid nanofluid flow across parallel surfaces.

As a result of Eq. (7), we get:

$$f'''' + \left(\frac{\rho_{hnf}}{\rho_f}\frac{\mu_f}{\mu_{hnf}}\right)Re\left(ff''' - f'f''\right) - 2R_0 g'\left(\frac{\rho_{hnf}}{\rho_f}\frac{\mu_f}{\mu_{hnf}}\right) - Mn\left(\frac{\sigma_{hnf}}{\sigma_f}\frac{\mu_f}{\mu_{hnf}}\right)f''g' = 0, \tag{8}$$

$$g'' + \left(\frac{\rho_{hnf}}{\rho_f}\frac{\mu_f}{\mu_{hnf}}\right)Re\left(fg' - f'g\right) - 2R_0\left(\frac{\rho_{hnf}}{\rho_f}\frac{\mu_f}{\mu_{hnf}}\right)g' - Mn\left(\frac{\mu_f}{\mu_{hnf}}\frac{\sigma_{hnf}}{\sigma_f}\right)g = 0, \tag{9}$$

$$\left(1 + \frac{4}{3}R_d\right)\frac{k_f}{k_{hnf}}\theta'' + \frac{(\rho c_p)_{hnf}}{(\rho c_p)_f}\frac{k_f}{k_{hnf}}Re\,Pr\,f\theta' + Hs\theta = 0. \tag{10}$$

The reduced conditions are:

$$\left.\begin{array}{l} f'(0) = 1,\; f(0) = \alpha,\; \theta(0) = 1,\; g(0) = 0 \quad \text{at} \quad \eta = 0, \\ f'(1) = \lambda,\; f(1) = \beta,\; \theta(1) = 0,\; g(1) = 0 \quad \text{at} \quad \eta = 1. \end{array}\right\} \tag{11}$$

Here $\beta = -\frac{v_L}{aL}$ and $\alpha = -\frac{v_0}{qL}$ are the injection and suction factors for upper and lower surfaces, $\lambda = \frac{b}{a}$ is the stretching factor, $Re = \frac{\sigma^*(T_2)^3}{k^* k_f}$ is the radiation factor, $Re = \frac{aL^2\rho_f}{\mu_f}$ is the Reynolds number, $Pr = \frac{Cp_f\mu_f}{k_f}$ is the Prandtl number, $R_0 = \frac{L^2\Omega\rho_f}{\mu_f}$ is the rotation constraint and $Mn = \frac{B_0^2 L^2\sigma_f}{\mu_f}$ magnetic term.

The physical interest quantities are:

$$C_f = \frac{-2\mu_{hnf}}{\rho_{hnf}u_0^2}\left.\frac{\partial u}{\partial y}\right|_{y=0}, \quad or \;\; C_f = -2\frac{\mu_{hnf}}{\mu_f}\frac{\rho_f}{\rho_{hnf}}f''(0). \tag{12}$$

$$Nu = \frac{-L}{k_f(T_0 - T_L)}\left(k_{hnf}\right)\left.\frac{\partial T}{\partial y}\right|_{y=0}, \quad or \;\; Nu = -\frac{k_{hnf}}{k_f}\theta'(0). \tag{13}$$

Numerical solution

A details explanation related to PCM methodology is followed[54–56]:

Step 1 Generalization to 1st order ODE

$$\bar{\lambda}_1 = f(\eta), \quad \bar{\lambda}_3 = f''(\eta), \quad \bar{\lambda}_5 = g(\eta), \quad \bar{\lambda}_7 = \theta(\eta), \\ \bar{\lambda}_2 = f'(\eta), \quad \bar{\lambda}_4 = f'''(\eta), \quad \bar{\lambda}_6 = g'(\eta), \quad \bar{\lambda}_8 = \theta'(\eta).$$
(14)

By putting Eq. (14) in Eqs. (8)–(10) and (11), we get:

$$\bar{\lambda}_4' + \frac{\rho_{hnf}}{\rho_f} \frac{\mu_f}{\mu_{hnf}} \text{Re}(\bar{\lambda}_1\bar{\lambda}_4 - \bar{\lambda}_2\bar{\lambda}_3) - 2R_0\bar{\lambda}_6 \frac{\rho_{hnf}}{\rho_f} \frac{\mu_f}{\mu_{hnf}} - Mn\frac{\sigma_{hnf}}{\sigma_f} \frac{\mu_f}{\mu_{hnf}} \bar{\lambda}_3\bar{\lambda}_6 = 0,$$
(15)

$$\bar{\lambda}_6' + \frac{\rho_{hnf}}{\rho_f} \frac{\mu_f}{\mu_{hnf}} \text{Re}(\bar{\lambda}_1\bar{\lambda}_6 - \bar{\lambda}_2\bar{\lambda}_5) - 2R_0 \frac{\rho_{hnf}}{\rho_f} \frac{\mu_f}{\mu_{hnf}} \bar{\lambda}_6 - Mn\frac{\mu_f}{\mu_{hnf}} \frac{\sigma_{hnf}}{\sigma_f} \bar{\lambda}_5 = 0,$$
(16)

$$\left(1 + \frac{4}{3}R_d\right) \frac{k_f}{k_{hnf}} \bar{\lambda}_8' + \frac{(\rho c_p)_{hnf}}{(\rho c_p)_f} \frac{k_f}{k_{hnf}} \text{Re Pr } \bar{\lambda}_1\bar{\lambda}_8 + Hs\bar{\lambda}_7 = 0.$$
(17)

The transform conditions are:

$$\bar{\lambda}_1(0) = \alpha, \quad \bar{\lambda}_2(0) = 1, \quad \bar{\lambda}_5(0) = 0, \quad \bar{\lambda}_7(0) = 1 \quad \text{at} \quad \eta = 0, \\ \bar{\lambda}_1(1) = \beta, \quad \bar{\lambda}_2(1) = \lambda, \quad \bar{\lambda}_5(1) = 0, \quad \bar{\lambda}_7(1) = 0 \quad \text{at} \quad \eta = 1.$$
(18)

Step 2 Introducing parameter *p* in Eq. (16)–(20):

$$\bar{\lambda}_4' + \frac{\rho_{hnf}}{\rho_f} \frac{\mu_f}{\mu_{hnf}} \text{Re}(\bar{\lambda}_1\bar{\lambda}_4 - \bar{\lambda}_2\bar{\lambda}_3) - 2R_0\bar{\lambda}_6 \frac{\rho_{hnf}}{\rho_f} \frac{\mu_f}{\mu_{hnf}} - Mn\frac{\sigma_{hnf}}{\sigma_f} \frac{\mu_f}{\mu_{hnf}} \bar{\lambda}_3\bar{\lambda}_6 = 0,$$
(19)

$$\bar{\lambda}_6' + \frac{\rho_{hnf}}{\rho_f} \frac{\mu_f}{\mu_{hnf}} \text{Re}(\bar{\lambda}_1\bar{\lambda}_6 - \bar{\lambda}_2\bar{\lambda}_5) - 2R_0 \frac{\rho_{hnf}}{\rho_f} \frac{\mu_f}{\mu_{hnf}} \bar{\lambda}_6 - Mn\frac{\mu_f}{\mu_{hnf}} \frac{\sigma_{hnf}}{\sigma_f} \bar{\lambda}_5 = 0,$$
(20)

$$\left(1 + \frac{4}{3}R_d\right) \frac{k_f}{k_{hnf}} \bar{\lambda}_8' + \frac{(\rho c_p)_{hnf}}{(\rho c_p)_f} \frac{k_f}{k_{hnf}} \text{RePr } \bar{\lambda}_1\bar{\lambda}_8 + Hs\bar{\lambda}_7 = 0.$$
(21)

Results and discussion

This segment expresses the physical mechanisms and reason behind the increasing and decreasing effect of velocity, mass, and energy outlines versus physical interest quantities. The following are some different profiles:

Velocity interpretation. Figures 2, 3, 4 and 5 describe the effect of the stretching parameter λ, Reynold number Re, rotation factor R_0, and suction parameter α on the radial velocity curve $f(\eta)$. Figures 2 and 3 show that the velocity field lessens with the varying values of stretching constraint λ and Reynold number Re. Physically, the constant stretching of the sheet generates disturbance, which resists the fluid motion and as a result drops the velocity curve $f(\eta)$ as revealed in Fig. 2. Similarly, from the mathematical expression of Reynold number Re $= \frac{aL^2\rho_f}{\mu_f}$, one can observe that the density and distance (L) between two surfaces increases with the effect
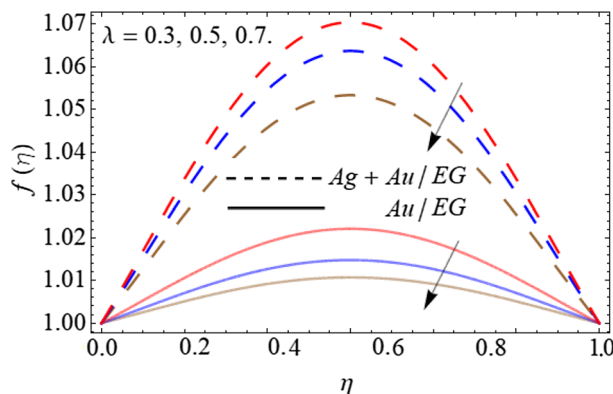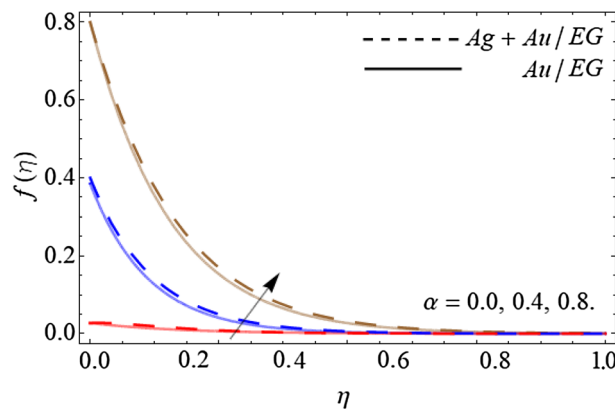

Figure 2. Consequence of the Stretching parameter λ on $f(\eta)$.
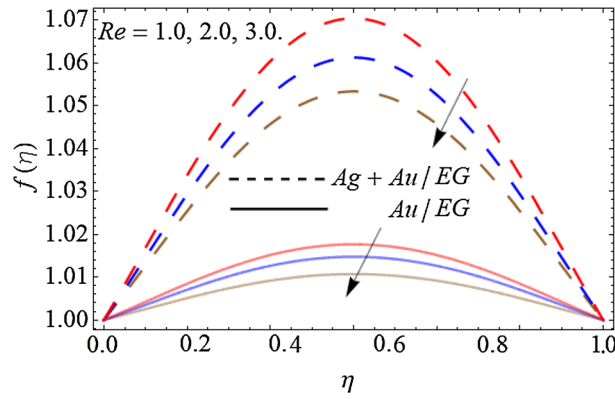
**Figure 3.** Consequence of the Reynold number Re on $f(\eta)$.
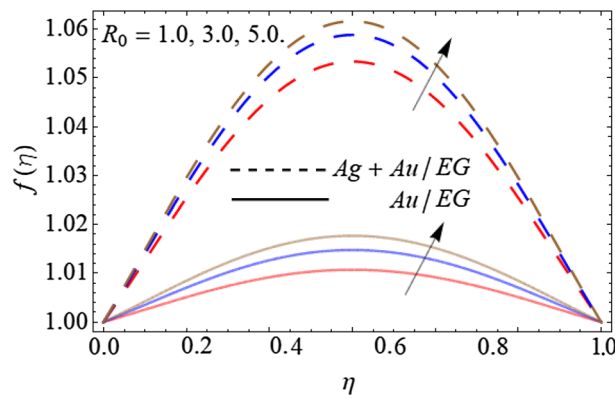
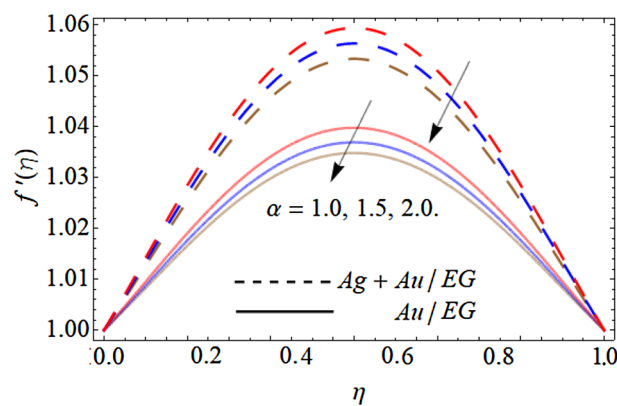**Figure 4.** Consequence of the Rotation factor R_0 on $f(\eta)$.

Figure 5. Consequence of the Suction term α on $f(\eta)$.

of Reynold number, which causes the reduction of velocity curve as presented in Fig. 3. Because the flow motion boots in the narrow tube or channel as compared to wide according to the Bernoulli statement. Figures 4 and 5 exhibit that the $f(\eta)$ deteriorates with the varying values of rotation factor R_0 and suction parameter α. Physically, the angular motion of surfaces, rotates the fluid particles adjacent to the surface according to the no-slip conditions and as a result, the velocity outline enhances as exposed in Fig. 4. Figure 5 expresses that the $f(\eta)$ develops with the upshot of suction factor.
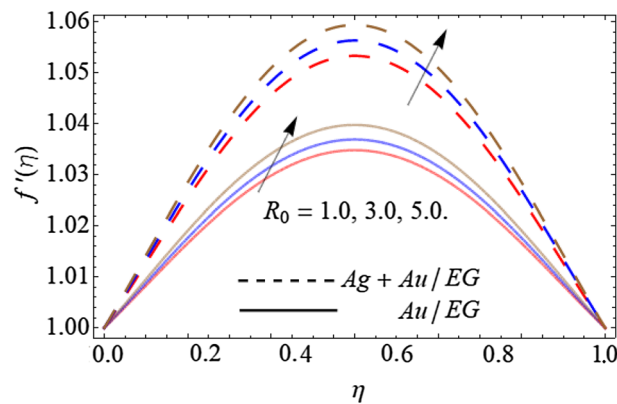
Figures 6, 7, 8 and 9 describe the effect injection parameter β, suction parameter α, rotation parameter β, and nanoparticles volume friction (ϕ_1, ϕ_2) on the axial velocity curve $f'(\eta)$ respectively. Figures 6 and 7 reveal
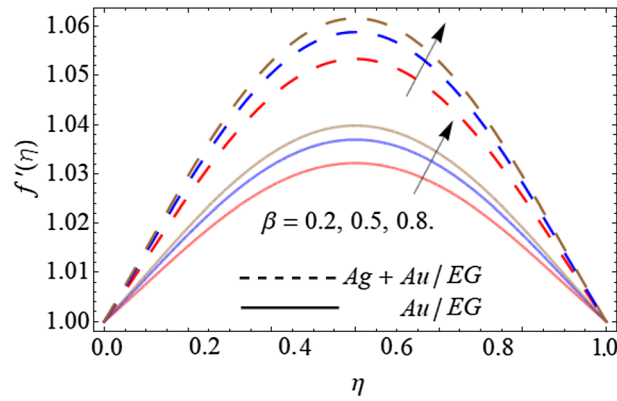
**Figure 6.** Consequence of the Injection parameter β on $f'(\eta)$.

**Figure 7.** Consequence of the Suction parameter α on $f'(\eta)$.

Figure 8. Consequence of the Rotation parameter β on $f'(\eta)$.

that the influence of the injection parameter β enhances, while the effect of the suction factor α drops the axial velocity curve $f'(\eta)$. Figures 8 and 9 expose that the growing values of the rotation term β and mounting numbers of nanoparticles (ϕ_1, ϕ_2) boost the velocity curve. As we have discoursed before that the angular motion of surfaces, rotates the fluid particles adjacent to the surface according to the no-slip conditions, hence, the velocity outline $f'(\eta)$ augments as publicized in Fig. 8. On the other hand, the specific heat capacity of ethylene glycol $\left(2430\,c_p\ \left(\text{J Kg}^{-1}\ \text{K}^{-1}\right)\right)$ is greater than the Au and Ag NPs. Therefore, the inclusion of Au and Ag NPs in EG reduces the heat-absorbing capacity of HNF, as a result, the fluid loses its viscosity and accelerates the fluid motion $f'(\eta)$ as revealed in Fig. 9.

7
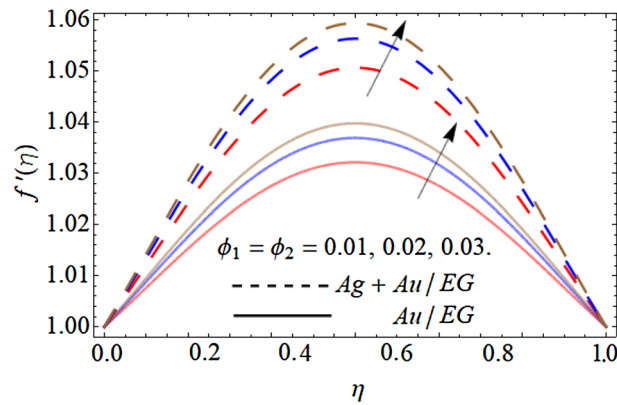
Figure 9. Consequence of the rising numbers of Nanoparticles on $f'(\eta)$.

Temperature interpretation. Figures 10, 11, 12 and 13 pronounce the effect of nanoparticles volume fric-tion (ϕ_1, ϕ_2), Reynold number Re, radiation term Rd and heat source Hs on the energy curve $\theta(\eta)$ respectively. Figure 10 expresses that the energy outline enhances with the rising number of Au and Ag NPs. Physically, the thermal conductivity of Ag and Au Nps is greater than EG, therefore, the addition of these NPs to EG, boosts the average thermal conductivity of hybrid nanoliquid as displayed in Fig. 10. Figure 11 shows that the varying influence of Reynold number diminishes the energy curve. Figures 12 and 13 illustrates that the energy curve $\theta(\eta)$ augments with the effect of thermal radiation term and heat source Hs. Physically, thermal radiation is the radiation produced by the thermal transfer of matter particulate. Thermal radiation is produced when the heat generated by charge mobility in content is transformed into electromagnetic radiation. This electromagnetic radiation, when applied to the fluid flow, accelerates the energy curve $\theta(\eta)$ as demonstrated in Fig. 12. Similarly, the heat source also enhances the energy outlines of the hybrid nanoliquid as presented in Fig. 13. Physically,
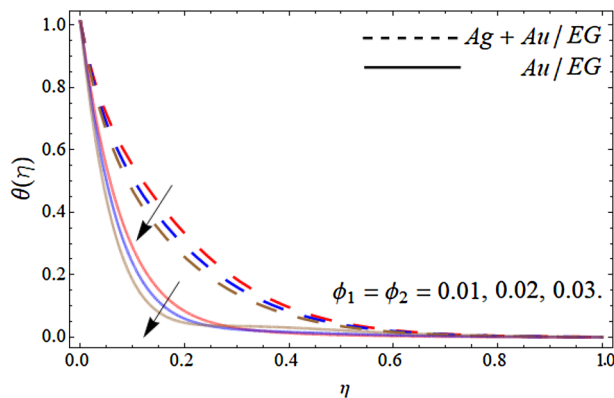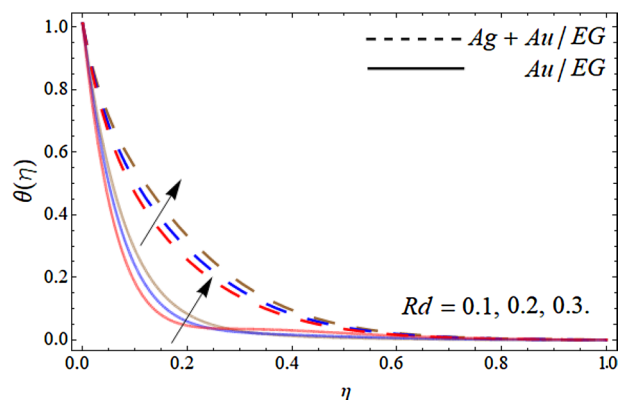

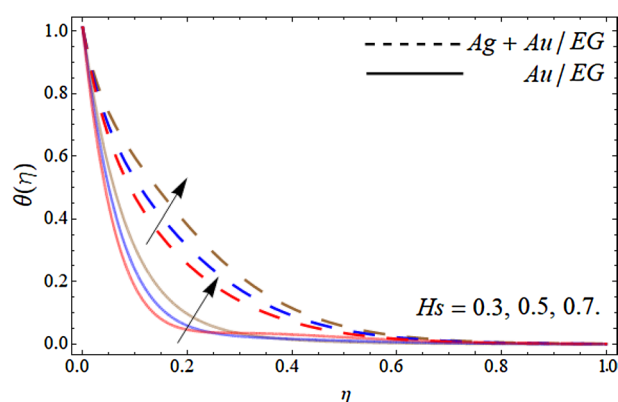**Figure 10.** Consequence of the rising numbers of Nanoparticles on the energy curve $\theta(\eta)$.
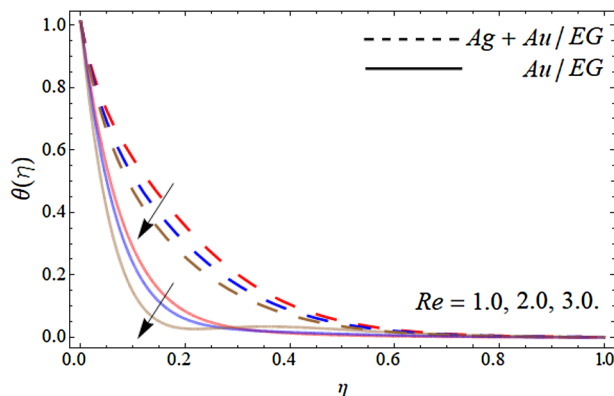
Figure 11. Consequence of the Reynold number Re on the energy curve $\theta(\eta)$.

Figure 12. Consequence of the Radiation term on the energy curve $\theta(\eta)$.

Figure 13. Consequence of the heat source on the energy curve $\theta(\eta)$.

Thermo-physical properties	Base fluid	Nanoparticles	
	$C_2H_6O_2$(Ethylene–Glycol)	Ag (Silver)	Au (Gold)
ρ (Kg m^{-3})	1115	10,500	19,300
c_p $(\text{J Kg}^{-1}\text{ K}^{-1}))$	2430	235	129.1
k $(\text{W m}^{-1}\text{ K}^{-1})$	0.253	429	318
$\beta \times 10^{-5}$ (K^{-1})	5.7	1.89	1.4
σ (S m^{-1})	10.7×10^{-5}	6.30×10^7	4.25×10^7

Table 1. The thermo-physical properties of nano particulates with base fluid[53].

the heat source/sink is a passive energy transport that communicates the energy fashioned by mechanical or an electronic apparatus into a coolant fluid in motion. The heat source is a source that radiates or generates heat.

Tables 1 and 2 elaborate the tentative values of Au-NPs and Ag-NPs and EG used for the simulation of the problem and mathematical model comprising different thermal features of the EG and nanoparticles. Table 3 expresses the comparative study of the present work against the published literature for validity purposes as well as revealed the statistical results for C_f and Nu. It can be perceived that both physical interest quantities $(C_f, \text{ Nu})$ transfer rate boost with the influence of Reynold number and NPs volume friction.

Conclusions

The analysis of energy and mass transport mechanism through the MHD spinning flow of an ethylene glycol based HNF across two permeable surfaces is reviewed. The hybrid nanofluid is made of Ag and Au-NPs in ethylene glycol. The solution obtained from the PCM is presented through Tables and Figures. The key conclusions are:

	Nanofluids	Hybrid-nanofluid $\phi_{hnf} = (\phi_{Ag} + \phi_{Au})$
Viscosity μ	$\frac{\mu_f}{(1-\phi_{Au})}$ and $\frac{\mu_f}{(1-\phi_{Ag})}$	$\frac{\mu_f}{(1-\phi_{hnf})^{2.5}}$
Density ρ	$(1-\phi_{Au})\rho f + \phi_{Au}\rho_{Au}$ and $(1-\phi_{Ag})\rho f + \phi_{Ag}\rho_{Ag}$	$(1-\phi_{hnf})\rho f + \phi_{Ag}\rho_{Ag} + \phi_{Au}\rho_{Au}$
Heat capacity (ρC_p)	$(1-\phi_{Au})(\rho C_p)_f + \phi_{Au}(\rho C_p)_{Au}$ and $(1-\phi_{Ag})(\rho C_p)_f + \phi_{Ag}(\rho C_p)_{Ag}$	$(1-\phi_{hnf})(\rho C_p)_f + \phi_{Ag}(\rho C_p)_{Ag} + \phi_{Au}(\rho C_p)_{Au}$
Thermal conductivity k	$\frac{k_{Au}+2k_f-2\phi_{Au}(k_f-k_{Au})}{k_{Au}+2k_f+2\phi_{Au}(k_f-k_{Au})}k_f$ and $\frac{k_{Ag}+2k_f-2\phi_{Ag}(k_f-k_{Ag})}{k_{Ag}+2k_f+2\phi_{Ag}(k_f-k_{Ag})}k_f$	$\frac{k_{Au}+2k_{nf}-2\phi_{Au}(k_{nf}-k_{Au})}{k_{Au}+2k_{nf}+2\phi_{Au}(k_{nf}-k_{Au})}$ $\times \frac{k_{Ag}+2k_f-2\phi_{Ag}(k_f-k_{Ag})}{k_{Ag}+2k_f+2\phi_{Ag}(k_f-k_{Ag})}k_f$
Diffusivity α	$\frac{k_{nf}}{(\rho C_p)_{nf}}$	$\frac{k_{hnf}}{(\rho C_p)_{hnf}}$

Table 2. The thermos-physical characteristics of HNF[53].

Parameters			Hafeez et al.[51]	Present work	Parameters			Hafeez et al.[51]	Present work
Re	R_0	Mn	C_f	C_f	Re	$\phi_1 = \phi_2$	Pr	Nu	Nu
1.0			71.9017	71.90181	1.0			14.0721	14.07223
2.0			74.0635	74.06362	2.0			15.1956	15.19572
3.0			**76.2852**	**76.28545**	**3.0**			**16.3696**	**16.36975**
	1.5		71.9054	71.90553			3.0	6.59670	6.596728
	2.0		71.9106	71.91076			4.0	14.0721	14.07238
	2.5		**71.9173**	**71.91751**			**5.0**	**38.2791**	**38.27936**
		2.5	72.0311	72.03138		2.5		4.43466	4.434689
		3.0	72.1601	72.16038		3.0		4.76439	4.764473
		3.5	**72.2890**	**72.28923**		**3.5**		**5.10782**	**5.107858**

Table 3. The statistical outcomes of skin friction and Nusselt number. Significant values are in [bold].

- The radial velocity curve declines with the varying values of the stretching parameter λ and Reynold number Re.
- The fluid velocity curve $f(\eta)$ drops with the variation of rotation factor R_0 and suction parameter while improving with the influence of the suction factor.
- The influence of the injection parameter β enhances, while the effect of the suction parameter α drops the axial velocity curve $f'(\eta)$.
- The rising values of rotation constraint β and mounting numbers of nanoparticles (ϕ_1, ϕ_2) boost the velocity curve.
- The energy framework enhances with the effect of thermal radiation term and heat source. The energy framework also enriches with the rising number of Au and Ag NPs in the base fluid.
- Both physical interest quantities (C_f, Nu) transfer rate boost with the influence of Reynold number and NPs volume friction.

Data availability
All data used in this manuscript have been presented within the article.

References
1. Acharya, N., Das, K. & Kundu, P. K. Rotating flow of carbon nanotube over a stretching surface in the presence of magnetic field: A comparative study. *Appl. Nanosci.* **8**(3), 369–378 (2018).
2. Dogonchi, A. S. *et al.* Investigation of magneto-hydrodynamic fluid squeezed between two parallel disks by considering Joule heating, thermal radiation, and adding different nanoparticles. *Int. J. Numer. Methods Heat Fluid Flow* **30**(2), 659–680 (2020).
3. Ahmadian, A., Bilal, M., Khan, M. A. & Asjad, M. I. The non-Newtonian maxwell nanofluid flow between two parallel rotating disks under the effects of magnetic field. *Sci. Rep.* **10**(1), 1–14 (2020).
4. Khan, M. I., Hafeez, M. U., Hayat, T., Khan, M. I. & Alsaedi, A. Magneto rotating flow of hybrid nanofluid with entropy generation. *Comput. Methods Programs Biomed.* **183**, 105093 (2020).
5. Krishna, M. V. & Chamkha, A. J. Hall and ion slip effects on MHD rotating flow of elastico-viscous fluid through porous medium. *Int. Commun. Heat Mass Transfer* **113**, 104494 (2020).
6. Islam, S. *et al.* Influences of Hall current and radiation on MHD micropolar non-Newtonian hybrid nanofluid flow between two surfaces. *AIP Adv.* **10**(5), 055015 (2020).

7. Fiza, M., Alsubie, A., Ullah, H., Hamadneh, N. N., Islam, S. & Khan, I. Three-dimensional rotating flow of MHD Jeffrey fluid flow between two parallel plates with impact of hall current. *Math. Probl. Eng.* (2021).
8. Shahzad, F., Jamshed, W., Sajid, T., Nisar, K. S. & Eid, M. R. Heat transfer analysis of MHD rotating flow of Fe_3O_4 nanoparticles through a stretchable surface. *Commun. Theor. Phys.* **73**(7), 075004 (2021).
9. Bilal, M., Ali, A., Hejazi, H.A. & Mahmuod, S.R. Numerical study of an electrically conducting hybrid nanofluid over a linearly extended sheet. *Z. Angew. Math. Mech.* e202200227 (2022).
10. Ali, F. *et al.* Effects of Newtonian heating and heat generation on magnetohydrodynamics dusty fluid flow between two parallel plates. *Front. Mater.* **10**, 1120963 (2023).
11. Yaseen, M., Rawat, S. K. & Kumar, M. Cattaneo–Christov heat flux model in Darcy–Forchheimer radiative flow of $MoS_2–SiO_2$/ kerosene oil between two parallel rotating disks. *J. Therm. Anal. Calorim.* **147**, 1–23 (2022).
12. Alqarni, M. M., Bilal, M., Allogmany, R., Tag-Eldin, E., Ghoneim, M. E. & Yassen, M. F. Mathematical analysis of Casson fluid flow with energy and mass transfer under the influence of activation energy from a non-coaxially spinning disc. *Front. Energy Res.* **10** (2022).
13. Alqahtani, A. M., Bilal, M., Usman, M., Alsenani, T. R., Ali, A. & Mahmuod, S. R. Heat and mass transfer through MHD Darcy Forchheimer Casson hybrid nanofluid flow across an exponential stretching sheet. *ZAMM-J. Appl. Math. Mech. /Zeitschrift für Angewandte Mathematik und Mechanik* e202200213 (2023).
14. Ramzan, M. *et al.* Hydrodynamic and heat transfer analysis of dissimilar shaped nanoparticles-based hybrid nanofluids in a rotating frame with convective boundary condition. *Sci. Rep.* **12**(1), 1–17 (2022).
15. Ali, S., Khan, A., Shah, K., Alqudah, M. A. & Abdeljawad, T. On computational analysis of highly nonlinear model addressing real world applications. *Results Phys.* **36**, 105431 (2022).
16. Haq, K., Shah, K., & Abdeljawad, T. (2022). Analysis of periodic heat transfer through extended surfaces. *Therm. Sci.* 184.
17. Haq, I. *et al.* Mixed convection nanofluid flow with heat source and chemical reaction over an inclined irregular surface. *ACS Omega* **7**, 30477–30485 (2022).
18. Alhowaity, A., Hamam, H., Bilal, M. & Ali, A. Numerical study of Williamson hybrid nanofluid flow with thermal characteristics past over an extending surface. *Heat Transf.* **51**(7), 6641–6655 (2022).
19. Nadeem, S., Abbas, N. & Malik, M. Y. Inspection of hybrid based nanofluid flow over a curved surface. *Comput. Methods Programs Biomed.* **189**, 105193 (2020).
20. Gul, T. *et al.* Magnetic dipole impact on the hybrid nanofluid flow over an extending surface. *Sci. Rep.* **10**(1), 1–13 (2020).
21. Tlili, I., Nabwey, H. A., Ashwinkumar, G. P. & Sandeep, N. 3-D magnetohydrodynamic AA7072-AA7075/methanol hybrid nanofluid flow above an uneven thickness surface with slip effect. *Sci. Rep.* **10**(1), 1–13 (2020).
22. Manzoor, U., Imran, M., Muhammad, T., Waqas, H. & Alghamdi, M. (2021). Heat transfer improvement in hybrid nanofluid flow over a moving sheet with magnetic dipole. *Waves Random Complex Media* 1–15.
23. Wahid, N. S., Arifin, N. M., Khashi'ie, N. S. & Pop, I. Marangoni hybrid nanofluid flow over a permeable infinite disk embedded in a porous medium. *Int. Commun. Heat Mass Transf.* **126**, 105421 (2021).
24. Waqas, H., Farooq, U., Naseem, R., Hussain, S. & Alghamdi, M. Impact of MHD radiative flow of hybrid nanofluid over a rotating disk. *Case Stud. Therm. Eng.* **26**, 101015 (2021).
25. Kumar, R. N. *et al.* Impact of magnetic dipole on ferromagnetic hybrid nanofluid flow over a stretching cylinder. *Phys. Scr.* **96**(4), 045215 (2021).
26. Chu, Y. M., Bashir, S., Ramzan, M. & Malik, M. Y. Model-based comparative study of magnetohydrodynamics unsteady hybrid nanofluid flow between two infinite parallel plates with particle shape effects. *Math. Methods Appl. Sci.* (2022).
27. Wang, J. *et al.* Simulation of hybrid nanofluid flow within a microchannel heat sink considering porous media analyzing CPU stability. *J. Pet. Sci. Eng.* **208**, 109734 (2022).
28. Eid, M. R. & Nafe, M. A. Thermal conductivity variation and heat generation effects on magneto-hybrid nanofluid flow in a porous medium with slip condition. *Waves Random Complex Media* **32**(3), 1103–1127 (2022).
29. Alqahtani, A. M. *et al.* Transport properties of two-dimensional dissipative flow of hybrid nanofluid with Joule heating and thermal radiation. *Sci. Rep.* **12**(1), 19374 (2022).
30. Tayebi, T. *et al.* Thermo-economic and entropy generation analyses of magnetic natural convective flow in a nanofluid-filled annular enclosure fitted with fins. *Sustain. Energy Technol. Assess.* **46**, 101274 (2021).
31. Chamkha, A. J., Dogonchi, A. S. & Ganji, D. D. Magnetohydrodynamic nanofluid natural convection in a cavity under thermal radiation and shape factor of nanoparticles impacts: A numerical study using CVFEM. *Appl. Sci.* **8**(12), 2396 (2018).
32. Seyyedi, S. M., Dogonchi, A. S., Hashemi-Tilehnoee, M., Ganji, D. D., & Chamkha, A. J. Second law analysis of magneto-natural convection in a nanofluid filled wavy-hexagonal porous enclosure. *Int. J. Numer. Methods Heat Fluid Flow* (2020).
33. Eshaghi, S. *et al.* The optimum double diffusive natural convection heat transfer in H-Shaped cavity with a baffle inside and a corrugated wall. *Case Stud. Therm. Eng.* **28**, 101541 (2021).
34. Dogonchi, A. S. *et al.* Thermal and entropy analyses on buoyancy-driven flow of nanofluid inside a porous enclosure with two square cylinders: Finite element method. *Case Stud. Therm. Eng.* **27**, 101298 (2021).
35. Afshar, S. R. *et al.* Dissection of entropy production for the free convection of NEPCMs-filled porous wavy enclosure subject to volumetric heat source/sink. *J. Taiwan Inst. Chem. Eng.* **128**, 98–113 (2021).
36. Pasha, A. A. *et al.* Efficacy of exothermic reaction on the thermal-free convection in a nano-encapsulated phase change materials-loaded enclosure with circular cylinders inside. *J. Energy Storage* **59**, 106522 (2023).
37. Khan, A., Ullah, S., Shah, K., Alqudah, M. A., Abdeljawad, T. & Ghani, F. Theory and semi-analytical study of micropolar fluid dynamics through a porous channel.
38. Bilal, M. *et al.* Parametric simulation of micropolar fluid with thermal radiation across a porous stretching surface. *Sci. Rep.* **12**(1), 1–11 (2022).
39. Algehyne, E. A. *et al.* Numerical simulation of bioconvective Darcy Forchhemier nanofluid flow with energy transition over a permeable vertical plate. *Sci. Rep.* **12**(1), 1–12 (2022).
40. Alharbi, K. A. M. *et al.* Computational valuation of darcy ternary-hybrid nanofluid flow across an extending cylinder with induction effects. *Micromachines* **13**(4), 588 (2022).
41. Salehi, S., Nori, A., Hosseinzadeh, K. & Ganji, D. D. Hydrothermal analysis of MHD squeezing mixture fluid suspended by hybrid nanoparticles between two parallel plates. *Case Stud. Therm. Eng.* **21**, 100650 (2020).
42. Alotaibi, H., Althubiti, S., Eid, M. R. & Mahny, K. L. Numerical treatment of mhd flow of casson nanofluid via convectively heated non-linear extending surface with viscous dissipation and suction/injection effects. *Comput. Mater. Continua* **66**(1), 229–245 (2020).
43. Wu, J. & Zhu, Y. Global solutions of 3D incompressible MHD system with mixed partial dissipation and magnetic diffusion near an equilibrium. *Adv. Math.* **377**, 107466 (2021).
44. Armaghani, T. *et al.* MHD mixed convection of localized heat source/sink in an Al2O3-Cu/water hybrid nanofluid in L-shaped cavity. *Alex. Eng. J.* **60**(3), 2947–2962 (2021).
45. Patil, V. S., Patil, A. B., Ganesh, S., Humane, P. P. & Patil, N. S. Unsteady MHD flow of a nano Powell-Eyring fluid near stagnation point past a convectively heated stretching sheet in the existence of chemical reaction with thermal radiation. *Mater. Today Proc.* **44**, 3767–3776 (2021).

46. Elayarani, M., Shanmugapriya, M. & Kumar, P. S. Intensification of heat and mass transfer process in MHD carreau nanofluid flow containing gyrotactic microorganisms. *Chem. Eng. Process. Process Intensif.* **160**, 108299 (2021).
47. Vishalakshi, A. B., Mahabaleshwar, U. S. & Sarris, I. E. An MHD fluid flow over a porous stretching/shrinking sheet with slips and mass transpiration. *Micromachines* **13**(1), 116 (2022).
48. Khashi'ie, N. S., Arifin, N. M. & Pop, I. Magnetohydrodynamics (MHD) boundary layer flow of hybrid nanofluid over a moving plate with Joule heating. *Alex. Eng. J.* **61**(3), 1938–1945 (2022).
49. Abdelhameed, T. N. Entropy generation of MHD flow of sodium alginate ($C_6H_9NAO_7$) fluid in thermal engineering. *Sci. Rep.* **12**(1), 1–14 (2022).
50. Kodi, R. & Mopuri, O. Unsteady MHD oscillatory Casson fluid flow past an inclined vertical porous plate in the presence of chemical reaction with heat absorption and Soret effects. *Heat Transf.* **51**(1), 733–752 (2022).
51. Hafeez, M. U., Hayat, T., Alsaedi, A. & Khan, M. I. Numerical simulation for electrical conducting rotating flow of Au (Gold)-Zn (Zinc)/EG (Ethylene glycol) hybrid nanofluid. *Int. Commun. Heat Mass Transf.* **124**, 105234 (2021).
52. Rauf, A., Shah, N. A. & Botmart, T. Hall current and morphological effects on MHD micropolar non-Newtonian tri-hybrid nanofluid flow between two parallel surfaces. *Sci. Rep.* **12**(1), 1–20 (2022).
53. Shamshuddin, M. D., Mabood, F. & Beg, O. A. Thermomagnetic reactive ethylene glycol-metallic nanofluid transport from a convectively heated porous surface with ohmic dissipation, heat source, thermophoresis and Brownian motion effects. *Int. J. Modell. Simul.* **42**, 782–796 (2021).
54. Shuaib, M., Shah, R. A., Durrani, I. & Bilal, M. Electrokinetic viscous rotating disk flow of Poisson–Nernst–Planck equation for ion transport. *J. Mol. Liq.* **313**, 113412 (2020).
55. Shuaib, M., Shah, R. A. & Bilal, M. Variable thickness flow over a rotating disk under the influence of variable magnetic field: An application to parametric continuation method. *Adv. Mech. Eng.* **12**(6), 1687814020936385 (2020).
56. Elattar, S. *et al.* Computational assessment of hybrid nanofluid flow with the influence of hall current and chemical reaction over a slender stretching surface. *Alex. Eng. J.* **61**(12), 10319–10331 (2022).

Acknowledgements

Author contributions

M.B. and A.A. wrote the original manuscript and performed the numerical simulation. A.M.A. and S.M.E. reviewed the mathematical results and restructured the manuscript. Also T.R.A. responses the reviewer's queries and validate the results. The validation, funding acquisitions and supervision belongs to S.M.E. All authors are agreed on the final draft of the submission file.

Competing interests

The authors declare no competing interests.

Additional information

Correspondence and requests for materials should be addressed to A.A. or S.M.E.

Reprints and permissions information is available at www.nature.com/reprints.

Publisher's note Springer Nature remains neutral with regard to jurisdictional claims in published maps and institutional affiliations.